Interactions between Diameter, Myelination and the Na/K pump Affect Axonal Resilience to High Frequency Spiking

Yunliang Zang & Eve Marder*

Volen Center and Department of Biology, Brandeis University, Waltham, MA 02454, USA

*marder@brandeis.edu

Keywords: computational model; action potential; node of Ranvier; electrogenic pumps; sodium dynamics

Running title: Axonal resilience to high frequency firing

Abstract

Axons reliably conduct action potentials between neurons and/or other targets. Axons have widely variable diameters and can be myelinated or unmyelinated. Although the effect of these factors on propagation speed is well studied, how they constrain axonal resilience to high frequency spiking is incompletely understood. Maximal firing frequencies range from ~ 1 Hz to > 300 Hz across

neurons, but the process by which Na/K pumps counteract Na^+ influx is slow, and it is unclear the extent to which slow Na^+ removal is compatible with high frequency spiking. Modeling the process of Na^+ removal in unmyelinated and myelinated axons shows that both increasing diameter and myelination slow down [Na^+] accumulation and increase axonal resilience to high frequency spiking. Increasing pump density alleviates [Na^+] accumulation, but can paradoxically reduce the resilience. We speculate that [Na^+] accumulation may contribute to fatigue after continuous high frequency firing.

Significance

The reliability of spike propagation in axons is determined by complex interactions between ionic currents, ion pumps and morphological properties. We use compartment-based modeling to uncover that interactions of diameter, myelination and the Na/K pump determine axonal resilience to high frequency spiking. The Na/K pump can play a double-edged sword role in affecting axonal excitability. Our findings suggest that slow sodium removal influences axonal resilience to high frequency spiking, and may also contribute to fatigue.

Introduction

Axons usually reliably conduct information (spikes) to other neurons, muscles and glands. The largest diameter axons are found in some invertebrates, where the squid giant axon and arthropod giant fibers are parts of rapid escape systems. In the mammalian nervous system, axon diameters can differ by a factor of > 100. Some are covered with myelin sheaths but others are not (1). Both myelination and large axon diameter increase spike propagation speed (2, 3), and the latter factor can also increase axonal resilience to noise perturbation (4).

Neuronal firing frequency is not static, but variations in firing rates are used to encode a wide range of signals such as inputs from sensory organs and command signals from motor cortex. The maximal firing frequency, critical for neuronal functional capacity, ranges from ~ 1 Hz to > 300 Hz (5-8). However, it remains unclear how axonal physical properties constrain axonal resilience to high frequency firing. During action potentials, Na^+ flows into axons and then ATP is used by Na/K pumps to pump out the excess Na^+. Given the limited energy supply in the brain, evolutionary strategies including shortening spike propagation distance, reducing Na^+- and K^+-current overlap, and sparse coding, etc. have helped minimize energy expenditure (9-13). However, the observation that high frequency spiking tends to occur in larger diameter axons is confusing because it exerts a heavy burden on the energy supply in the brain (5, 14, 15). Additionally, the process by which Na/K pumps remove Na^+ is slow (16-22). In neurons, it takes seconds or even minutes to remove the excess Na^+ after Na^+ elevation (16-21). It remains unknown how these directly correlated processes, fast spiking and slow Na^+ removal, interact in the control of reliable spike generation and propagation. Consequently, by modeling the process of Na^+ removal in

unmyelinated and myelinated axons, we systematically explored the effects of diameter, myelination and Na/K pump density on spiking reliability.

Results

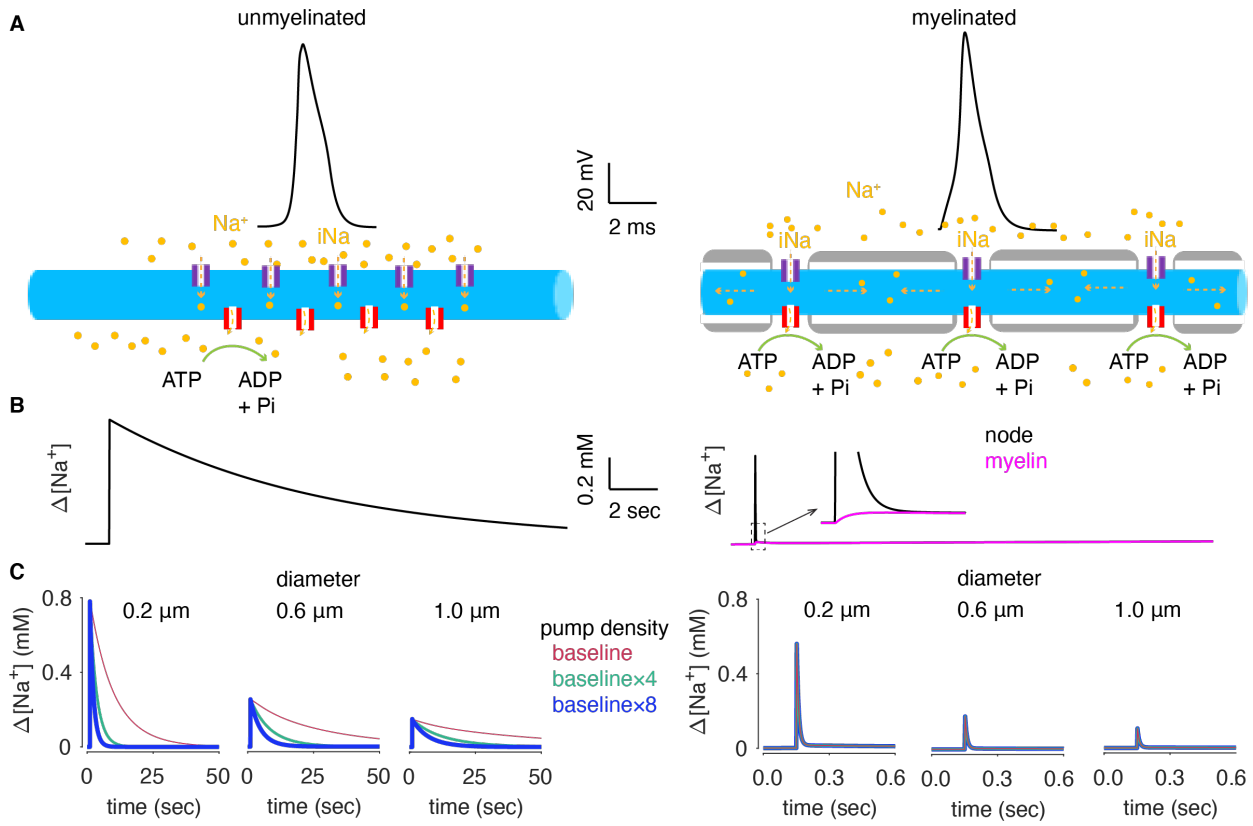

Fig. 1. Spike-triggered [Na^+] rise and decay in unmyelinated and myelinated axon models. (A) Schematic of the unmyelinated (left) and the myelinated (right) axon models. Black traces show spike waveforms recorded at the center of each model. (B) Spike-triggered [Na^+] rise and decay in the unmyelinated (left) and the myelinated (right) axon models. In the unmyelinated axon model, [Na^+] was recorded at the center of the axon. In the myelinated axon model, [Na^+] at the central node of Ranvier and the myelinated compartment (10.5 µm far) are shown. Initial parts of [Na^+] changes are enlarged in the inset. The Na/K pump density is 0.5 pmol/cm^2, referred to as baseline condition hereafter. (C) The effects of diameter and pump density on [Na^+] rise and decay in the unmyelinated (left) and the myelinated (right) axon models. Note the very different time scales for results in the two models.

Different [Na^+] Decay Dynamics in Unmyelinated and Myelinated Axons. We implemented multicompartment model of axons in NEURON (23). Both unmyelinated and myelinated axon

71 models include I_{Na}, I_{KD}, I_{KA}, I_{leak} and the Na/K pump. All channels and pumps were evenly spread
72 in the unmyelinated axon model and at the nodes of Ranvier in the myelinated axon model. For
73 the myelinated compartments, there is a significantly lower density of I_{leak} and C_m to simulate the
74 effect of insulation (Methods). The model structures are shown in Fig. 1A.

75 Spikes propagate rapidly in both models. In the unmyelinated axon model, the propagation
76 increases from 0.16 m/s to 0.39 m/s when the axonal diameter increases from 0.2 μm to 1 μm. In
77 the myelinated axon model, the speed increases from 2.5 m/s to 10 m/s accordingly. Upon the
78 arrival of spikes, Na^+ channels open and extracellular Na^+ flows into axons to raise the intracellular
79 [Na^+] immediately (Fig. 1B). Then K^+ currents are activated to repolarize the spikes. Compared
80 with the other ionic currents, the magnitude of the Na/K pump current is extremely small during a
81 single spike, but it decays very slowly. Eventually, the Na/K pump gradually removes Na^+ from
82 the axon, leading to a slow, many second, [Na^+] decay in the unmyelinated axon model (Fig. 1B,
83 left). In contrast, in the myelinated axon model, the spike-triggered [Na^+] elevation at the node of
84 Ranvier decays on the time scale of hundreds of ms (Fig. 1B, right). The Na/K pump densities in
85 two models are the same and thus the quick decay is not a result of super-efficient pumps. In the
86 myelinated axon model, Na^+ channels are placed only in the nodes of Ranvier and there is no Na^+
87 influx in myelinated compartments. But, the slightly elevated [Na^+] in the myelinated compartment
88 and the rapid decay of nodal [Na^+] are due to the axial diffusion of Na^+ into neighboring myelinated
89 compartments, rather than immediate pump action.

90 Because of the large diffusion coefficient (24) and the lack of buffering (16), [Na^+] in the radial
91 direction becomes rapidly homogeneous. Thus, spike-triggered [Na^+] elevation can be well
92 predicted by the surface-to-volume ratio (SVR $\propto$ 1/diameter). In both models, spike-triggered [Na^+]
93 elevation decreases with diameter (Fig. 1C). Increasing the pump density speeds up the [Na^+]

decay in the unmyelinated axon model, but has no obvious effect on the nodal [Na^+] decay in the myelinated axon model, further confirming that the quick decay is not a result of the Na/K pump.

[Na^+] Accumulation in the Unmyelinated Axon at High Firing Frequencies. Compared with the basal level before spiking (~ 10 mM), the [Na^+] elevation caused by a single spike is small and insufficient to affect axonal excitability (Fig. 1B). However, neurons can fire at high frequencies when animals receive stimuli or undergo behavior changes (7, 25-27). With continuous high frequency spiking, [Na^+] can accumulate if subsequent spikes occur before the complete recovery of a preceding spike elicited [Na^+] rise. In the unmyelinated axon model, [Na^+] significantly accumulates within just 100 spikes, and the accumulation speed increases with firing frequency because of a faster Na^+ influx rate (Fig. 2A, above). Larger SVRs also make [Na^+] accumulate faster in thin axons. In parallel with [Na^+] accumulation, the Na^+ reversal potential (driving force of Na^+ current) becomes more negative and the spike amplitude decreases (Fig. 2A, middle and bottom).

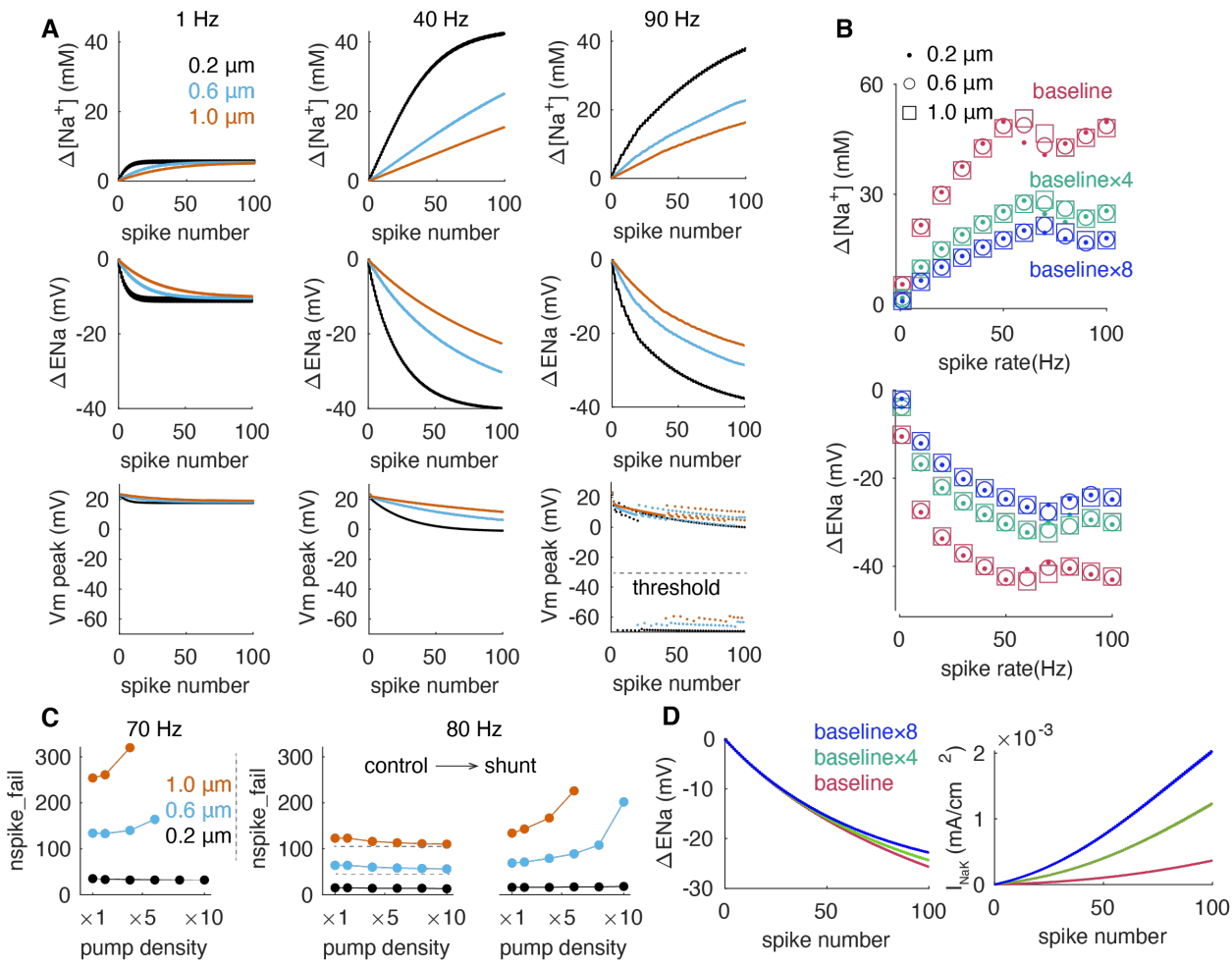

Fig. 2. The effects of diameter and pump density on [Na^+] accumulation and resilience to high frequency spiking in the unmyelinated axon model. (A) The course of [Na^+] accumulation (above), Na^+ reversal potential decrease (middle) and membrane potential peak reduction (bottom) in models with different diameters (0.2, 0.6 and 1.0 µm) and firing frequencies (1, 40 and 90 Hz). Spike threshold is -30 mV. Na/K pump density is 0.5 pmol/cm^2 (baseline). (B) Steady state [Na^+] accumulation (above) and Na^+ reversal potential reduction (bottom) at different firing frequencies. Symbol codes diameter and color codes pump density. (C) The effect of pump density on the resilience to high frequency spiking, measured by the number of spikes required to cause spike failure (nspike_fail), when firing at 70 and 80 Hz. 'shunt' corresponds to neutral pumps, meaning pumps remove Na^+, but carry 0 net current. The absence of data points means spikes don't fail. (D) The course of Na^+ reversal potential decrease (left) and outward pump current increase (right) with different pump densities. Diameter is 0.6 µm and firing frequency is 80 Hz.

When the model fires over a sufficiently long period, Na^+ influx rate decreases and efflux rate increases because of elevated [Na^+]. Eventually, Na^+ influx rate and efflux rate balance each other and [Na^+] reaches a steady state. The steady state [Na^+] increases with firing frequency until the

occurrence of spike failure at high frequencies (Fig. 2B). Within the low frequency range, the steady state [Na^+] is independent of diameter despite different accumulation speeds. The rate of Na^+ influx per surface area is only determined by the firing frequency because of identical Na^+ channel density. The Na/K pump-caused net Na^+ efflux rate is determined by $-3k_1[pump][Na^+]^3 + 3k_2[pumpNa]$ (Methods). Because pump density is also identical, the model needs identical [Na^+] to match influx rate and reach a steady state irrespective of diameters. Na^+ influx rate becomes diameter dependent when spiking fails at high frequencies. Accordingly, different [Na^+] are required to reach a steady state. Increasing pump density can reduce [Na^+] accumulation and alleviate the reversal potential decrease, because the Na^+ efflux rate becomes larger (Fig. 2B).

As a result of incomplete recovery from inactivation of Na^+ channels and the accumulated [Na^+], spikes fail intermittently at high frequencies. This gradual occurrence of failure is alleviated in the absence of [Na^+] accumulation (data not shown). An example of spike failure is shown in Fig. 2A when the models fire at 90 Hz. [Na^+] accumulates slowly in thick axons and in thick axons it always requires more spikes to trigger spike failure than in thin axons, demonstrating that thick axons are more resilient to high frequency firing (Fig. 2A, C). At higher frequencies, [Na^+] accumulates faster and Na^+ channels recover less from inactivation. Consequently, fewer spikes are required to trigger spike failure and accordingly the resilience (equivalent to excitability) decreases (Fig. 2C).

Surprisingly, although increasing pump density alleviates [Na^+] accumulation, it doesn't consistently increase the resilience (Fig. 2C). We tested the pump density in the range of 1–10 times of the baseline level (0.5 pmol/cm^2). Increasing pump density doesn't obviously affect the resilience of the 0.2-μm-thick axon model. Although the resilience of 0.6- and 1.0-μm-thick axons

148 is increased by pump density at 70 Hz, their resilience decreases with pump density at 80 Hz.
149 When removing excess Na^+, the pumps carry a negative current. More pumps alleviate [Na^+]
150 accumulation and the resultant reversal potential decrease, but they also provide a larger outward
151 current to decrease the axonal excitability directly (Fig. 2D). To confirm that the larger outward
152 current accounts for the paradoxical effect of pump density on the resilience, we 'shunt' the pump
153 current (net current becomes neutral instead of outward, but still pumps out Na^+). After shunting
154 this current, increasing pump density consistently increases the resilience (an example at 80 Hz is
155 given in Fig. 2C). Thus, the effect of pump density on the resilience depends on the balance
156 between [Na^+] accumulation and increased outward current.

157

158 **Myelination Slows down [Na^+] accumulation.** In contrast to the slow decay of [Na^+] in the
159 unmyelinated axon, [Na^+] at the node of Ranvier in the myelinated axon shows a quick decay (Fig.
160 1B). Can nodal [Na^+] accumulate at high firing frequencies? It does accumulate to reduce the Na^+
161 reversal potential and spike amplitude peak in parallel (Fig. 3A). As explained previously, the
162 quick decay of nodal [Na^+] is a result of dilution, rather than being removed: nodal Na^+ influx
163 quickly diffuses into neighboring myelinated compartments. The diluted [Na^+] is still higher than
164 the pre-spiking level (Fig. 3A at 1 Hz, inset). Nodal Na^+ influx not only needs to fill the nodes of
165 Ranvier, but also the neighboring myelinated compartments, which is equivalent to decreasing the
166 SVR. Consequently, nodal [Na^+] still accumulates, but at a much slower speed. Compared with
167 the unmyelinated axon model, the [Na^+] elevation and the Na^+ reversal potential decrease are
168 negligible for 100 spikes in the myelinated axon model (Fig. 3B). Instead, it requires thousands of
169 spikes to significantly change nodal [Na^+]. Therefore, by acting like an 'anti-flood water reservoir',
170 myelin slows down the nodal [Na^+] accumulation and the excitability reduction.

Similar to the unmyelinated axon model, nodal [Na^+] accumulates faster at higher firing frequencies (Fig, 3A). Although the [Na^+] accumulation speed decreases with diameter, the steady

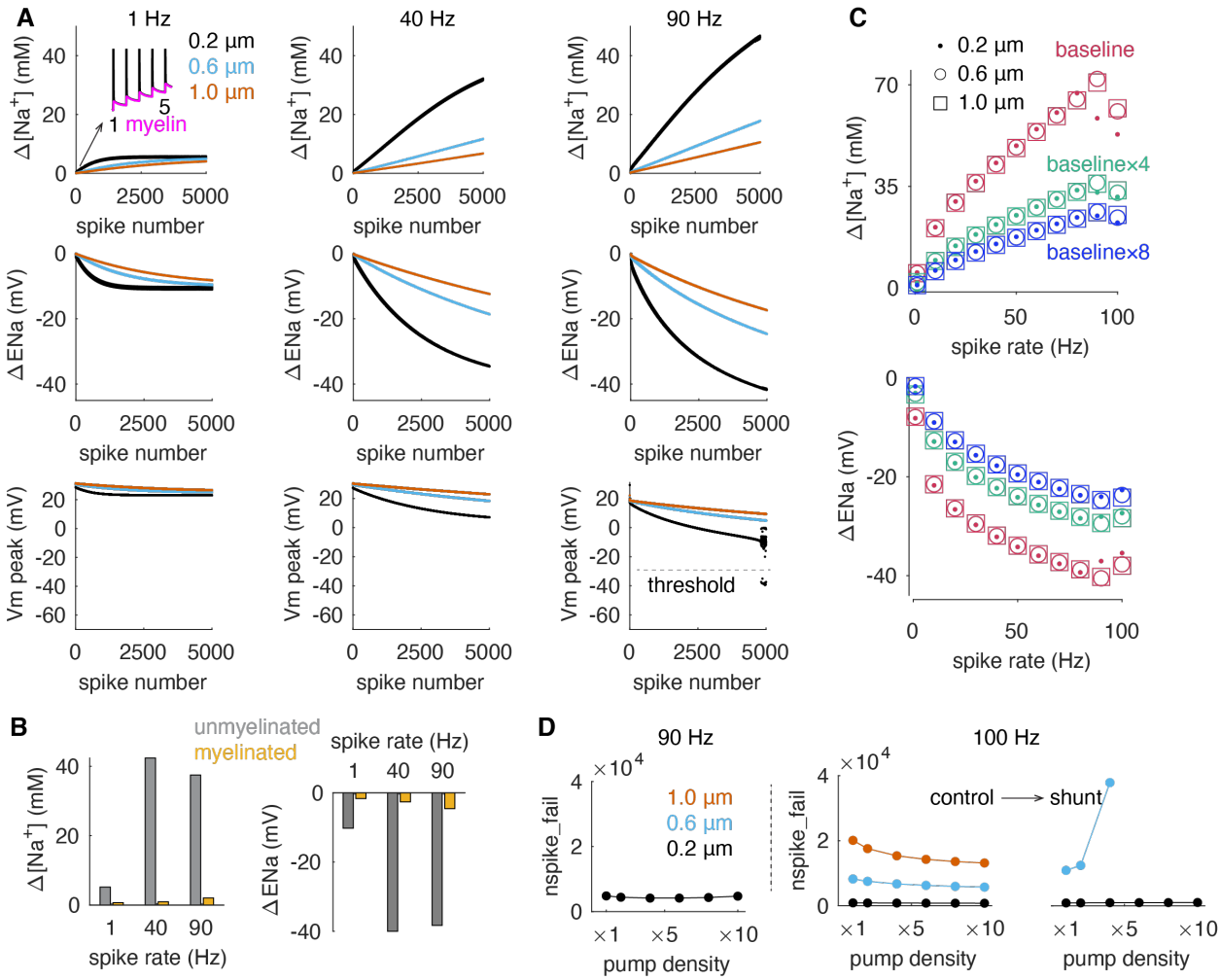

Fig. 3. Myelination slows down [Na^+] accumulation to increase the axonal resilience to high frequency spiking. (A) The course of [Na^+] accumulation (above), Na^+ reversal potential decrease (middle) and membrane potential peak reduction (bottom) at the node of Ranvier in the myelinated axon model with different diameters (0.2, 0.6 and 1.0 μm) and firing frequencies (1, 40 and 90 Hz). Fig. 2A shows 100 spike caused changes, but here shows 5000 spike caused changes. At 1 Hz, the [Na^+] in myelinated compartment (10.5 μm far) is also enlarged and shown in the inset when the diameter is 0.2 μm. Spike threshold is -30 mV. (B) 100-spike caused [Na^+] accumulation (left) and Na^+ reversal potential decrease (right) in the unmyelinated axon and the myelinated axon (node of Ranvier), with diameter of 0.2 μm. In A and B, the Na/K pump density is 0.5 pmol/cm^2 (baseline). (C) Steady state [Na^+] elevation (above) and Na^+ reversal potential decrease (bottom) at different firing frequencies. Symbol codes diameter and color codes pump density. (D) The effect of pump density on the axonal resilience to high frequency spiking, measured by the number of spikes required to cause spike failure (nspike_fail), when firing at 90 and 100 Hz. 'shunt' corresponds to neutral pumps. The absence of data points means spikes don't fail.

188
189
190 state [Na^+] is diameter independent until the occurrence of intermittent spike failure at high
191 frequencies (Fig. 3C). The [Na^+] accumulation and the Na^+ reversal potential decrease can be
192 alleviated by increasing pump density. Thick axons are consistently more resilient to high
193 frequency spiking (Fig. 3D). Still, increasing pump density doesn't consistently increase resilience,
194 but a consistent increase can be achieved by shunting the pump current.

195 Discussion

196 Neuronal firing frequency often varies over a broad range to encode a wide range of signals. For
197 a given neuron, its maximal firing frequency is usually much higher than the speed at which
198 intracellular Na^+ is pumped out of the cell. Therefore, while short periods of high frequency firing
199 should present no problem for most neurons, continuous high frequency spiking could result in
200 compromised function, as intracellular [Na^+] accumulates. Hence, we explore the dynamic
201 relationships between fast spiking and slow Na^+ removal for reliable spike generation and
202 propagation.

203 The importance of the Na/K ATPase in regulating neuronal activities has been called into
204 attention in recent years (28). It can set neuronal excitability and contribute to maintaining
205 synchronous epileptiform bursting in developing CA3 neurons (29). By interacting with h-current,
206 it regulates bursting activity in the leech heartbeat central pattern generator (30). There have also
207 been theoretical efforts to study the pump's role in controlling the transition between different
208 firing patterns (31-33) and the transition between normal and pathological brain states (34-36).
209 However, to the best of our knowledge, how the pump interacts with axon diameter and myelin to
210 remove [Na^+] influx and affect axonal excitability hasn't been explored previously.

211 Axonal morphology can exert a critical constraint on a neuron's maximal firing frequency.
212 Thick and myelinated axons are more resilient to high frequency spiking, because of their slow
213 [Na^+] accumulation and the resultant modest excitability reduction. In thin unmyelinated axons,
214 spiking may still be reliable at low frequencies owing to limited [Na^+] accumulation and
215 excitability reduction, but the reliability may be severely reduced when the axons fire at high
216 frequencies. This may explain why high frequency spiking tends to occur in thick axons, despite a
217 higher energetical cost of information transmission (5, 14).

218 Increasing the Na/K pump density to remove Na^+ more efficiently is expected to facilitate axonal
219 resilience to high frequency spiking. Existing data argue that Na^+ removal after spiking is slow.
220 For example, in axon initial segments of L5 pyramidal neurons, as a result of Na^+ diffusing into
221 the soma and myelin wrapped compartments, elevated [Na^+] requires several seconds to roughly
222 recover (16). In mitral cell tuft dendrites, after a short period of high frequency stimulation, it takes
223 minutes for the Na/K ATPase to pump out the Na^+ influx (17). This slow [Na^+] removal may be
224 functionally important because it enables integration and binding of multiple chemosensory stimuli
225 over a prolonged time scale (37). We used pump densities that should fall into a reasonable
226 biological range, and the [Na^+] accumulation at high firing frequencies shown here is consistent
227 with recent Na^+ imaging data (17, 20). Importantly, according to these simulation results,
228 increasing pumping efficiency is a two-edged sword. On the one hand, it does alleviate [Na^+]
229 accumulation; on the other hand, it reduces axonal excitability by carrying a larger outward current.

230 This work illustrates the limitations of using conventional frequency-current curves generated
231 with a short-term current injection to estimate the reliability of spike propagation (38, 39). Neither
232 of these measures reflects the accommodation of neuronal excitability after continuous firing

233 caused changes such as [Na^+] (explored in this work) and [Ca^{2+}] accumulation (showing a biphasic
234 decay (40, 41)).

235 In the models explored here, [Na^+] accumulation caused spike failure starting at 60 Hz in
236 unmyelinated axons. Specifically, when the axon diameter was 0.2 μm with the pump density of
237 0.5 pmol/cm^2, 1.1 sec continuous firing (66 spikes) elicited spike failure because of [Na^+]
238 accumulation. If only several spikes are required to encode a signal at this frequency, then [Na^+]
239 accumulation is unlikely to be an issue. However, with less recovery from inactivation of Na^+
240 channels at higher frequencies, spike failure reduces to 0.5 sec at 70 Hz (35 spikes), 0.19 sec at 80
241 Hz (15 spikes), 0.06 sec at 90 Hz (5 spikes) and 0.03 sec at 100 Hz (3 spikes).

242 In these modeled myelinated axons, spike failure was seen starting at 90 Hz. Specifically, when
243 the axon diameter was 0.2 μm with the pump density of 0.5 pmol/cm^2, failure only occurred after
244 continuous firing for 54 sec at 90 Hz (4821 spikes) and 8.7 sec at 100 Hz (873 spikes). Given that
245 myelinated axons are usually much thicker (1, 42), spike propagation in myelinated axons should
246 be extremely robust to fast firing caused [Na^+] accumulation under usual physiological conditions.
247 However, under conditions requiring neurons to fire for extended time at high frequencies, [Na^+]
248 accumulation may still compromise the function of axons. Of course, the frequency threshold and
249 the number of spikes required to cause spike failure will depend on the specifics of the expression
250 of neuronal conductances, and will likely show variability as a consequence of variable channel
251 densities (43). Additionally, intrinsic channel noise can cause spike failure (4), and the normal
252 function of the Na/K ATPases requires ATP, the supply of which has a limit (35). Both a shortage
253 of ATP after continuous firing and channel noise can further reduce axonal excitability.
254 Interestingly, a recent study observed intermittent spike propagation failure *in vivo* in dorsal root

ganglia of mice during sustained tactile stimuli (27). [Na^+] accumulation may be another important factor causing the failure apart from the channel noise.

Axon diameters can be up to 20 μm in the human peripheral nervous system and 1.5 mm in squid giant axons (1). For larger diameter axons, the conclusions still hold, because increasing diameter just further slows down [Na^+] accumulation. The localization of Na/K pumps in myelinated axons is still controversial (1, 44, 45). The paradoxical effect of pump density on the axonal resilience to high frequency spiking is preserved even if pumps are distributed between nodes of Ranvier (data not shown), as additive pumps increase the leakiness of the internodal compartments to reduce nodal excitability.

Fatigue is a deeply mysterious property that we all experience, and undoubtedly involves numerous cellular mechanisms (46). Significant [Na^+] accumulation has been observed in muscle cells and contributes to muscle fatigue after intense exercise (47, 48). Likewise, it is interesting to speculate that [Na^+] accumulation that occurs as a consequence of concerted and sustained neuronal activity could contribute to fatigue as we experience it.

ACKNOWLEDGMENTS. The authors would like to thank the constructive suggestions from the members of Marder lab. This work was supported by the grant R35NS097343.

References

1. S. G. Waxman, J. D. Kocsis, P. K. Stys, *The Axon: Structure, Function, and Pathophysiology* (Oxford University Press, 1995).
2. D. Debanne, E. Campanac, A. Bialowas, E. Carlier, G. Alcaraz, Axon physiology. Physiol Rev **91**, 555-602 (2011).
3. H. Schmidt, T. R. Knosche, Action potential propagation and synchronisation in myelinated axons. PLoS Comput Biol **15**, e1007004 (2019).
4. A. A. Faisal, J. A. White, S. B. Laughlin, Ion-channel noise places limits on the miniaturization of the brain's wiring. Curr Biol **15**, 1143-1149 (2005).
5. J. A. Perge, J. E. Niven, E. Mugnaini, V. Balasubramanian, P. Sterling, Why do axons differ in caliber? J Neurosci **32**, 626-638 (2012).

282 6. B. Wang *et al.*, Firing Frequency Maxima of Fast-Spiking Neurons in Human, Monkey, and
283 Mouse Neocortex. Front Cell Neurosci **10**, 239 (2016).
284 7. S. Chen, G. J. Augustine, P. Chadderton, Serial processing of kinematic signals by
285 cerebellar circuitry during voluntary whisking. Nat Commun **8**, 232 (2017).
286 8. A. Hasenstaub, S. Otte, E. Callaway, T. J. Sejnowski, Metabolic cost as a unifying principle
287 governing neuronal biophysics. Proc Natl Acad Sci USA **107**, 12329-12334 (2010).
288 9. S. B. Laughlin, Energy as a constraint on the coding and processing of sensory information.
289 Curr Opin Neurobiol **11**, 475-480 (2001).
290 10. W. B. Levy, R. A. Baxter, Energy efficient neural codes. Neural Comput **8**, 531-543 (1996).
291 11. H. Alle, A. Roth, J. R. Geiger, Energy-efficient action potentials in hippocampal mossy
292 fibers. Science **325**, 1405-1408 (2009).
293 12. F. J. Heras, J. Anderson, S. B. Laughlin, J. E. Niven, Voltage-dependent K^+ channels improve
294 the energy efficiency of signalling in blowfly photoreceptors. J R Soc Interface **14** (2017).
295 13. H. Hu, F. C. Roth, D. Vandael, P. Jonas, Complementary Tuning of Na^+ and K^+ Channel
296 Gating Underlies Fast and Energy-Efficient Action Potentials in GABAergic Interneuron
297 Axons. Neuron **98**, 156-165 e156 (2018).
298 14. C. Howarth, P. Gleeson, D. Attwell, Updated energy budgets for neural computation in
299 the neocortex and cerebellum. J Cereb Blood Flow Metab **32**, 1222-1232 (2012).
300 15. R. Nortley, D. Attwell, Control of brain energy supply by astrocytes. Curr Opin Neurobiol
301 **47**, 80-85 (2017).
302 16. I. A. Fleidervish, N. Lasser-Ross, M. J. Gutnick, W. N. Ross, Na^+ imaging reveals little
303 difference in action potential-evoked Na^+ influx between axon and soma. Nat Neurosci
304 **13**, 852-860 (2010).
305 17. A. Zylbertal, A. Kahan, Y. Ben-Shaul, Y. Yarom, S. Wagner, Prolonged Intracellular Na^+
306 Dynamics Govern Electrical Activity in Accessory Olfactory Bulb Mitral Cells. PLoS Biol **13**,
307 e1002319 (2015).
308 18. A. Zylbertal, Y. Yarom, S. Wagner, The Slow Dynamics of Intracellular Sodium
309 Concentration Increase the Time Window of Neuronal Integration: A Simulation Study.
310 Front Comput Neurosci **11**, 85 (2017).
311 19. D. Ziemens, F. Oschmann, N. J. Gerkau, C. R. Rose, Heterogeneity of Activity-Induced
312 Sodium Transients between Astrocytes of the Mouse Hippocampus and Neocortex:
313 Mechanisms and Consequences. J Neurosci **39**, 2620-2634 (2019).
314 20. T. Ona-Jodar, N. J. Gerkau, S. Sara Aghvami, C. R. Rose, V. Egger, Two-Photon Na^+ Imaging
315 Reports Somatically Evoked Action Potentials in Rat Olfactory Bulb Mitral and Granule Cell
316 Neurites. Front Cell Neurosci **11**, 50 (2017).
317 21. B. Moshrefi-Ravasdjani, D. Ziemens, N. Pape, M. Färfers, C. R. Rose, Action Potential Firing
318 Induces Sodium Transients in Macroglial Cells of the Mouse Corpus Callosum. Neuroglia
319 **1**, 106-125 (2018).
320 22. Y. Zang *et al.*, Theoretical investigation of the mechanism of heart failure using a canine
321 ventricular cell model: especially the role of up-regulated CaMKII and SR Ca^{2+} leak. J Mol
322 Cell Cardiol **56**, 34-43 (2013).
323 23. M. L. Hines, N. T. Carnevale, The NEURON simulation environment. Neural Comput **9**,
324 1179-1209 (1997).

24. M. J. Kushmerick, R. J. Podolsky, Ionic mobility in muscle cells. Science **166**, 1297-1298 (1969).
25. L. S. Tang *et al.*, Precise temperature compensation of phase in a rhythmic motor pattern. PLoS Biol **8**, e1000469 (2010).
26. J. C. Athilingam, R. Ben-Shalom, C. M. Keeshen, V. S. Sohal, K. J. Bender, Serotonin enhances excitability and gamma frequency temporal integration in mouse prefrontal fast-spiking interneurons. Elife **6**, e31991 (2017).
27. D. Al-Basha, S. A. Prescott, Intermittent Failure of Spike Propagation in Primary Afferent Neurons during Tactile Stimulation. J Neurosci **39**, 9927-9939 (2019).
28. M. D. Forrest, The sodium-potassium pump is an information processing element in brain computation. Frontiers in Physiology **5** (2014).
29. L. R. Shao, R. Janicot, C. E. Stafstrom, Na^+-K^+-ATPase functions in the developing hippocampus: regional differences in CA1 and CA3 neuronal excitability and role in epileptiform network bursting. J Neurophysiol **125**, 1-11 (2021).
30. D. Kueh, W. H. Barnett, G. S. Cymbalyuk, R. L. Calabrese, Na^+/K^+ pump interacts with the h-current to control bursting activity in central pattern generator neurons of leeches. Elife **5**, e19322 (2016).
31. M. D. Forrest, M. J. Wall, D. A. Press, J. Feng, The sodium-potassium pump controls the intrinsic firing of the cerebellar Purkinje neuron. PLoS One **7**, e51169 (2012).
32. A. O. Komendantov, C. C. Canavier, Electrical coupling between model midbrain dopamine neurons: effects on firing pattern and synchrony. J Neurophysiol **87**, 1526-1541 (2002).
33. C. C. Canavier, Sodium dynamics underlying burst firing and putative mechanisms for the regulation of the firing pattern in midbrain dopamine neurons: a computational approach. J Comput Neurosci **6**, 49-69 (1999).
34. G. P. Krishnan, G. Filatov, A. Shilnikov, M. Bazhenov, Electrogenic properties of the Na^+/K^+ ATPase control transitions between normal and pathological brain states. J Neurophysiol **113**, 3356-3374 (2015).
35. G. Le Masson, S. Przedborski, L. F. Abbott, A computational model of motor neuron degeneration. Neuron **83**, 975-988 (2014).
36. J. S. Coggan, G. K. Ocker, T. J. Sejnowski, S. A. Prescott, Explaining pathological changes in axonal excitability through dynamical analysis of conductance-based models. J Neural Eng **8**, 065002 (2011).
37. A. Zylbertal, Y. Yarom, S. Wagner, Synchronous Infra-Slow Bursting in the Mouse Accessory Olfactory Bulb Emerge from Interplay between Intrinsic Neuronal Dynamics and Network Connectivity. J Neurosci **37**, 2656-2672 (2017).
38. N. W. Gouwens *et al.*, Classification of electrophysiological and morphological neuron types in the mouse visual cortex. Nat Neurosci **22**, 1182-1195 (2019).
39. A. Foust, M. Popovic, D. Zecevic, D. A. McCormick, Action Potentials Initiate in the Axon Initial Segment and Propagate through Axon Collaterals Reliably in Cerebellar Purkinje Neurons. The Journal of Neuroscience **30**, 6891-6902 (2010).
40. H. Schmidt, K. M. Stiefel, P. Racay, B. Schwaller, J. Eilers, Mutational analysis of dendritic Ca^{2+} kinetics in rodent Purkinje cells: role of parvalbumin and calbindin D28k. J Physiol **551**, 13-32 (2003).

41. Y. Zang, S. Dieudonne, E. De Schutter, Voltage- and Branch-Specific Climbing Fiber Responses in Purkinje Cells. Cell Rep **24**, 1536-1549 (2018).
42. S. Lee *et al.*, A culture system to study oligodendrocyte myelination processes using engineered nanofibers. Nat Methods **9**, 917-922 (2012).
43. D. J. Schulz, J. M. Goaillard, E. Marder, Variable channel expression in identified single and electrically coupled neurons in different animals. Nat Neurosci **9**, 356-362 (2006).
44. S. G. Waxman, J. M. Ritchie, Molecular dissection of the myelinated axon. Ann Neurol **33**, 121-136 (1993).
45. E. A. Young *et al.*, Imaging correlates of decreased axonal Na^+/K^+ ATPase in chronic multiple sclerosis lesions. Ann Neurol **63**, 428-435 (2008).
46. J. J. Wan, Z. Qin, P. Y. Wang, Y. Sun, X. Liu, Muscle fatigue: general understanding and treatment. Exp Mol Med **49**, e384 (2017).
47. S. P. Cairns, M. I. Lindinger, Do multiple ionic interactions contribute to skeletal muscle fatigue? J Physiol **586**, 4039-4054 (2008).
48. T. Clausen, Quantification of Na^+,K^+ pumps and their transport rate in skeletal muscle: functional significance. J Gen Physiol **142**, 327-345 (2013).
49. Y. Zhang, D. Bucher, F. Nadim, Ionic mechanisms underlying history-dependence of conduction delay in an unmyelinated axon. Elife **6**, e25382 (2017).

Methods

Axonal Morphology. We modeled a segment of axon with the length of 303 μm. The model was implemented in NEURON (23). The model code will be available from ModelDB. The simulations used an integration step of 0.01 ms. The unmyelinated model was discretized into 15 segments in the longitudinal direction. Vm and [Na^+] were recorded at the central segment. For the myelinated axon model, there are 3 nodes of Ranvier flanked with 4 myelinated compartments (Figure 1). The lengths of the nodes of Ranvier are 1 μm (nseg = 1). The middle two myelinated compartments are 100 μm long each (nseg = 5 each) and the other two myelinated compartments are 50 μm each (nseg = 3 each). Vm and [Na^+] were recorded at the central node and its neighboring myelinated compartment. In the radial direction, there are 4 shells to model Na^+ diffusion (23). The Na^+ diffusion coefficient is 0.6 μm^2/ms (24) and there is no buffering (16), leading to a homogeneous [Na^+] in the radial direction. In both peripheral and central nervous systems, unmyelinated axons

are usually thinner than myelinated axons. In the central nervous system, axons > 0.2 μm are usually myelinated (1). To delineate the effect of both diameter and myelination on [Na^+] accumulation, we chose the same range of diameters between 0.2–1.0 μm.

Ionic Channels and the Na/K pump. The model has a minimal set of ionic channels: fast Na current (I_{Na}), delayed rectifier K current (I_{KD}), A-type K current (I_{KA}) and leak current (I_{leak}). They have standard kinetic formulations in the form of $I = g_{max} m^p h^q (V - E)$; $\tau_m \dot{m} = m_\infty(V) - m$; $\tau_h \dot{h} = h_\infty(V) - h$; g_{max} represents maximal conductance; m and h represent activation and inactivation gates; p and q represent corresponding gate exponents; E represents reversal potential; τ_m and τ_h represent corresponding time constants; All the channel kinetics were modified from (49). For I_{Na}, $g_{max} = 0.015\, S/cm^2$; $p = 3$; $q = 1$; $m_\infty = 1/(1 + exp(-(V + 38)/8.5))$; $\tau_m = 0.132/(\cosh((V + 27)/7.5) + 0.003/(1 + \exp(-(V + 27)/5)))$; $h_\infty = 1/(1 + exp(V + 47/6))$; $\tau_h = 10/cosh((V + 42)/15)$; $E_{Na} = RT/F * \ln([Na^+]_o/[Na^+]_i)$; $[Na^+]_o$ is fixed to be 140 mM; $[Na^+]_i$ (also written as [Na^+] in the main text) was dynamically computed by I_{Na} and the Na/K pump; For I_{KD}, $g_{max} = 0.216\, S/cm^2$; $p = 4$; $q = 0$; $m_\infty = (-0.01 * (V + 45.7)/(exp(-(V + 45.7)/10) - 1))/((-0.01 * (V + 45.7)/(exp(-(V + 45.7)/10) - 1)) + 0.125 * exp(-(V + 55.7)/80))$; $\tau_m = 1/((-0.01 * (V + 45.7)/(exp(-(V + 45.7)/10) - 1)) + 0.125 * exp(-(V + 55.7)/80))$; E_K = -70 mV; For I_{KA}, $g_{max} = 0.02\, S/cm^2$; $p = 3$; $q = 1$; $m_\infty = (0.0761 * exp((V + 94.22)/31.84)/(1 + exp((V + 1.17)/28.93)))^{1/3}$; $\tau_m = 0.3632 + 1.158/(1 + exp((V + 55.96)/20.12))$; $h_\infty = 1/\left(1 + exp(V + 53.3/14.54)\right)^4$; $\tau_h = 1.24 + 2.678/(1 + exp((V + 50)/16.027))$; For I_{leak}, $g_{max} = 1.25 \times 10^{-4}\, S/cm^2$; $p = 0$; $q = 0$; E_{leak} = -65 mV; the Na/K pump model is similar with that used in (17, 37), described by the following kinetic schemes: $[pump] + 3[Na^+]_i$

$\overset{k_1,k_2}{\longleftrightarrow}[pumpNa]$; $[pumpNa] \overset{k_3,k_4}{\longleftrightarrow} [pump] + 3[Na^+]_o$; $pump_{total} = [pump] + [pumpNa]$; $k_1 = 2\ mM^{-3}msec^{-1}$; $k_2 = 0.001\ msec^{-1}$; $k_3 = 0.6\ msec^{-1}$; $k_4 = 0.437\ mM^{-3}msec^{-1}$; By these parameters, the steady state $[Na^+]$ is ~ 10 mM when the axon models are silent.

For the unmyelinated axon model, all defined currents and the Na/K pump were evenly distributed with C_m = 1 μF/cm^2 and R_a = 120 Ωcm. For the myelinated axon model, the ionic currents and the Na/K pump were placed in the nodes of Ranvier (1, 44). For simplicity, we did not model juxtaparanodal regions. At the nodes of Ranvier, C_m = 1 μF/cm^2; On myelinated compartments, there is only a smaller I_{leak} with g_{max} = 1.25×10^{-6} S/cm^2 and effective C_m = 0.01 μF/cm^2; R_a is 120 Ωcm. In both the unmyelinated and the myelinated axon models, the current densities are identical so that we could explore the role of diameter and myelination on Na^+ accumulation. The $pump_{total}$ is in the range of 0.5–5 pmol/cm^2. To show the effect of outward pump current on axonal excitability, in Fig. 2 and 3, we 'shunt' the pump current by making it neural, which means it carries 0 net current. In the unmyelinated axon model, spikes were triggered by stimulating the left end to -30 mV when Na current was blocked; In the myelinated axon model, spikes were triggered by stimulating the first node of Ranvier to -30 mV when Na^+ current was blocked.